

Supporting Information for The rational construction of diamond-like dysprosium-hexacyanometallate frameworks featuring dynamic magnetic behaviour

Ai-Huan Sun,^{‡*a*} Xi-Xi Liu,^{‡*a*} Rong Sun,^{*b*} Jin Xiong,^{*b*} Hao-Ling Sun,^{**a*} and Song Gao^{**b*}

^{*a*} Department of Chemistry and Beijing Key Laboratory of Energy Conversion and Storage Materials, Beijing Normal University, Beijing 100875, P. R. China. E-mail: haolingsun@bnu.edu.cn;

^{*b*} Beijing National Laboratory for Molecular Sciences, State Key Laboratory of Rare Earth Materials Chemistry and Applications, College of Chemistry and Molecular Engineering, Peking University, Beijing 100871, P. R. China. E-mail: gaosong@pku.edu.cn;

‡ These authors contributed equally.

Experimental Section

X-ray crystallography and physical measurement

Intensity data for crystals of **1-4** were collected on a rigaku SuperNova, Dual, AtlasS2 diffractometer with graphite-monochromated Cu K α ($\lambda = 1.54059 \text{ \AA}$) radiation at 100 K. Using Olex2, the structure was solved with the olex2.solve structure solution program using Charge Flipping and refined with the olex2.refine refinement package using Gauss-Newton minimisation. All non-hydrogen atoms were refined anisotropically. Hydrogen atoms were placed at the calculation positions. The details of crystallographic data and selected bond parameters for complexes **1-4** are listed in Table S1†. CCDC 2109922-2109925 contain the supplementary crystallographic data for this paper.

The Fourier transform infrared (FT-IR) spectra were recorded using KBr pellets in the range of 4000 to 400cm⁻¹ on an AVATAR 360 Nicolet 380 FT/IR spectrometer. Elemental analyses (C, H, N) were implemented on an Elementar Vario EL analyzer. Thermogravimetric analyses (TGA) were carried out using a Mettler-Toledo TGA/DSC1 in air flow, from 30 °C to 1000 °C with a heating rate of 5 °C/min. Powder X-ray diffraction (PXRD) analyses were performed on a Rigaku Dmax-2000 X-ray diffractometer with Cu K α ($\lambda=1.54059$ Å) radiation. Variable-temperature magnetic susceptibility measurements of **1-4** were performed on Quantum Design PPMS magnetometer (100~10000 Hz) and Quantum Design SQUID-MPMS3 (1~1000 Hz) magnetometer.

Computational details

Complete-active-space self-consistent field (CASSCF) calculations on the Dy³⁺ ion fragment of compounds **2** and **4** on the basis of X-ray determined geometry have been carried out with *MOLCAS* 8.1 program package. For Complexes **2** and **4**, there is only one type of Dy³⁺ ion, and thus we only need to calculate one Dy³⁺ ion fragment. During the calculations, the other Dy³⁺ ion was replaced by diamagnetic Lu³⁺ ion, and the diamagnetic Co³⁺ ions were omitted, the model structure as show in Fig. S21†.

For CASSCF calculations, the basis sets for all atoms are atomic natural orbitals from the MOLCAS ANO-RCC library: ANO-RCC-VTZP for Dy³⁺ ion; VTZ for close O and N; VDZ for distant atoms. The calculations employed the second order Douglas-Kroll-Hess Hamiltonian, where scalar relativistic contractions were taken into account in the basis set and the spin-orbit coupling was handled separately in the restricted active space state interaction (RASSI-SO) procedure. For the fragment of Dy³⁺ ion, the active electrons in 7 active spaces include all *f* electrons CAS (9, 7) for complexes **2** and **4** in the CASSCF calculation. To exclude all the doubts, we calculated all the roots in the active space. We have mixed the maximum number of spin-free state which was possible with our hardware (all from 21 sextets, 128 from 224 quadruplets and 130 from 490 doublets for Dy³⁺ ion fragments).

Fitting the exchange interaction in complex **2** and **4** using Lines model based on CASSCF results

To fit the exchange interaction in complexes **2** and **4**, we took two steps to obtain them. Firstly, we calculated one Dy³⁺ ion fragment using CASSCF to obtain the corresponding magnetic properties. Then, the exchange interaction between the magnetic centres is considered within the Lines model, while the account of the dipole-dipole magnetic coupling is treated exactly. The Lines model is effective and has been successfully used widely in the research field of f-element single-molecule magnets.

For complexes **2** and **4**, there is only one type of J . The exchange Hamiltonian is:

$$\hat{H}_{exch} = -J^{total} \hat{S}_{Dy1} \hat{S}_{Dy2}$$

The J_{total} is the parameter of the total magnetic interaction ($J_{total} = J_{dipolar} + J_{exchange}$) between Dy³⁺ ions. The $\hat{S}_{Dy} = \pm 1/2$ is the ground pseudospin on the Dy³⁺ ion site. The dipolar magnetic coupling can be calculated exactly, while the exchange coupling constant was fitted through comparison of the computed and measured magnetic susceptibility using the POLY_ANISO program.

Table S1 Selected bond lengths (Å) and bond angles (°) in complexes **1-4**

Bond length	1	2	3	4
Dy1-O1	2.205(3)	2.201(2)	2.185(3)	2.185(2)
Dy1-O2	2.387(3)	2.384(2)	2.403(2)	2.405(2)
Dy1-O2#1	2.319(2)	2.318(2)	2.320(2)	2.322(2)
Dy1-O3	2.391(3)	2.392(2)	2.459(2)	2.399(2)
Dy1-O4	2.443(3)	2.432(2)	2.397(2)	2.455(2)
Dy1-N1#1	2.541(3)	2.537(3)	2.508(2)	2.526(2)
Dy1-N3	2.483(3)	2.481(3)	2.384(2)	2.501(2)
Dy1-N4	2.391(3)	2.398(3)	2.525(2)	2.388(2)
Dy1-Dy1#1	3.959(1)	3.958(3)	3.944(5)	3.946(3)
Dy1-Fe1	5.438(1)	-	5.419(3)	-
Bond angle	1	2	3	4
O1-Dy1-O2	136.8(1)	137.1(8)	134.6(7)	134.6(6)
O1-Dy1-O2#1	154.6(1)	154.2(3)	154.3(7)	153.9(7)
Dy1-O2-Dy1#1	114.6(2)	114.7(2)	113.2(2)	113.2(1)

Symmetry code for **1**: #1 -x+1/2, -y+1/2, -z+1/2; **2**: #1 -x+2, -y+1, -z+1; **3**: #1 -x+1/2, -y+1/2, -z+1/2; **4**: #1 -x+1/2, -y+3/2, -z+3/2.

Table S2. Relaxation fitting parameters from Least-Squares Fitting of $\chi(f)$ data under zero dc field of 1.

T/K	χ_T	χ_S	α	τ (s)
2	36.98	0.23	0.11	1.63E-3
2.5	28.95	0.44	0.09	1.43E-3
3	23.68	0.45	0.08	1.31E-3
3.5	19.91	0.42	0.08	1.22E-3
4	17.15	0.37	0.08	1.14E-3
4.5	15.00	0.39	0.08	1.07E-3
5	13.32	0.39	0.08	1.01E-3
5.5	11.97	0.39	0.08	9.60E-4
6	10.85	0.41	0.07	9.15E-4
6.5	9.93	0.40	0.07	8.74E-4
7	9.15	0.39	0.07	8.36E-4
7.5	8.48	0.41	0.06	7.96E-4
8	7.90	0.40	0.06	7.56E-4
8.5	7.39	0.41	0.06	7.11E-4
9	6.94	0.42	0.05	6.64E-4
9.5	6.56	0.40	0.05	6.13E-4
10	6.20	0.39	0.05	5.60E-4
10.5	5.88	0.37	0.05	5.05E-4
11	5.60	0.36	0.05	4.54E-4
11.5	5.34	0.36	0.04	4.03E-4
12	5.10	0.12	0.06	3.50E-4
12.5	4.87	0.37	0.04	3.15E-4
13	4.68	0.10	0.07	2.69E-4
13.5	4.51	0.10	0.06	2.33E-4
14	4.33	0.10	0.06	2.00E-4
14.5	4.05	0.11	0.04	1.76E-4
15	3.90	0.11	0.04	1.51E-4
15.5	3.77	0.11	0.03	1.31E-4
16	3.63	0.11	0.03	1.13E-4
16.5	3.53	0.10	0.04	9.68E-5
17	3.42	0.10	0.04	8.32E-5
17.5	3.31	0.10	0.03	7.13E-5
18	3.21	0.11	0.03	6.08E-5
18.5	3.12	0.10	0.03	5.20E-5
19	3.03	0.10	0.03	4.43E-5
19.5	2.96	0.07	0.05	3.71E-5
20	2.87	0.11	0.03	3.18E-5
20.5	2.79	0.12	0.03	2.71E-5
21	2.72	0.12	0.03	2.28E-5
21.5	2.66	0.06	0.04	1.85E-5

Table S3. Relaxation fitting parameters from Least-Squares Fitting of $\chi(f)$ data under zero dc field of 2.

T/K	χ_T	χ_S	α	$\tau(s)$
5	13.44	0.08	0.08	0.13
5.5	12.08	0.08	0.07	0.10
6	10.94	0.08	0.06	0.07
6.5	9.97	0.08	0.06	0.05
7	9.16	0.07	0.05	0.04
7.5	8.48	0.07	0.05	0.03
8	7.87	0.07	0.05	0.02
8.5	7.37	0.07	0.05	0.01
9	6.93	0.07	0.05	8.63E-3
9.5	6.50	0.07	0.04	6.19E-3
10	6.14	0.07	0.04	4.52E-3
10.5	5.83	0.07	0.04	3.34E-3
11	5.54	0.07	0.04	2.51E-3
11.5	5.28	0.08	0.04	1.91E-3
12	5.03	0.08	0.04	1.47E-3
12.5	4.82	0.08	0.04	1.14E-3
13	4.63	0.08	0.04	8.95E-4
13.5	4.43	0.12	0.04	7.13E-4
14	4.30	0.05	0.05	5.81E-4
14.5	4.11	0.16	0.03	4.61E-4
15	3.99	0.04	0.06	3.77E-4
15.5	3.81	0.30	0.01	3.16E-4
16	3.72	0.04	0.06	2.48E-4
16.5	3.60	0.04	0.06	2.02E-4
17	3.46	0.05	0.05	1.64E-4
17.5	3.38	0.03	0.07	1.33E-4
18	3.24	0.06	0.05	1.09E-4
18.5	3.15	0.06	0.05	8.84E-5
19	3.07	0.06	0.05	7.22E-5
19.5	2.98	0.06	0.05	5.87E-5
20	2.91	0.06	0.06	4.75E-5
20.5	2.81	0.10	0.04	3.93E-5
21	2.74	0.09	0.05	3.19E-5
21.5	2.68	0.12	0.04	2.64E-5
22	2.61	0.15	0.04	2.18E-5
22.5	2.55	0.13	0.05	1.77E-5

Table S4. Relaxation fitting parameters from Least-Squares Fitting of $\chi(f)$ data under zero dc field of **3**.

T/K	χ_T	χ_S	α	τ (s)
2	35.70	1.18	0.11	9.15E-4
2.5	28.45	1.71	0.09	7.44E-4
3	23.06	1.54	0.08	6.50E-4
3.5	19.17	1.25	0.08	5.83E-4
4	16.43	1.16	0.08	5.33E-4
4.5	14.37	1.11	0.07	4.92E-4
5	12.74	1.13	0.07	4.58E-4
5.5	11.44	1.07	0.07	4.27E-4
6	10.37	1.09	0.07	4.02E-4
6.5	9.49	1.02	0.07	3.76E-4
7	8.73	0.99	0.07	3.54E-4
7.5	8.08	1.01	0.07	3.35E-4
8	7.53	1.04	0.06	3.18E-4
8.5	7.05	0.93	0.07	2.95E-4
9	6.61	1.00	0.06	2.82E-4
9.5	6.23	1.02	0.05	2.66E-4
10	5.89	0.93	0.06	2.42E-4
10.5	5.61	0.19	0.12	2.33E-4
11	5.33	0.17	0.12	2.13E-4
11.5	5.08	0.17	0.12	1.91E-4
12	4.85	0.16	0.12	1.72E-4
12.5	4.65	0.15	0.12	1.56E-4
13	4.42	0.17	0.10	1.40E-4
13.5	4.24	0.17	0.10	1.25E-4
14	4.13	0.17	0.08	1.19E-4
14.5	3.92	0.17	0.08	1.05E-4
15	3.78	0.17	0.08	9.24E-5
15.5	3.64	0.17	0.07	8.16E-5
16	3.52	0.17	0.07	7.17E-5
16.5	3.40	0.17	0.07	6.30E-5
17	3.29	0.18	0.06	5.52E-5
17.5	3.19	0.19	0.06	4.86E-5
18	3.10	0.19	0.06	4.25E-5
18.5	3.00	0.20	0.05	3.72E-5
19	2.92	0.16	0.07	3.19E-5
19.5	2.83	0.17	0.06	2.81E-5
20	2.75	0.24	0.04	2.42E-5
20.5	2.69	0.10	0.08	2.08E-5

Table S5. Relaxation fitting parameters from Least-Squares Fitting of $\chi(f)$ data under zero dc field of 4.

T/K	χ_T	χ_S	α	$\tau(s)$
5	13.51	0.06	0.15	0.07
5.5	12.16	0.06	0.15	0.06
6	10.98	0.06	0.14	0.04
6.5	9.96	0.06	0.13	0.03
7	9.11	0.06	0.12	0.02
7.5	8.39	0.06	0.11	0.01
8	7.75	0.06	0.10	0.01
8.5	7.22	0.06	0.09	9.03E-3
9	6.75	0.07	0.08	9.49E-3
9.5	6.36	0.07	0.08	4.72E-3
10	5.99	0.07	0.07	3.48E-3
10.5	5.70	0.07	0.08	2.61E-3
11	5.42	0.08	0.07	1.98E-3
11.5	5.21	0.07	0.09	1.52E-3
12	4.94	0.10	0.07	1.17E-3
12.5	4.72	0.13	0.07	9.20E-4
13	4.53	0.15	0.06	7.30E-4
13.5	4.34	0.18	0.06	5.86E-4
14	4.18	0.04	0.08	4.69E-4
14.5	4.01	0.27	0.04	3.90E-4
15	3.89	0.03	0.09	3.05E-4
15.5	3.74	0.32	0.04	2.63E-4
16	3.62	0.04	0.09	2.02E-4
16.5	3.45	0.05	0.07	1.61E-4
17	3.39	0.03	0.10	1.32E-4
17.5	3.24	0.07	0.07	1.11E-4
18	3.13	0.08	0.06	9.16E-5
18.5	3.05	0.09	0.06	7.52E-5
19	2.96	0.09	0.07	6.16E-5
19.5	2.89	0.09	0.07	5.03E-5
20	2.79	0.13	0.06	4.20E-5
20.5	2.72	0.16	0.05	3.47E-5
21	2.64	0.19	0.04	2.90E-5
21.5	2.59	0.15	0.06	2.32E-5
22	2.52	0.20	0.05	1.96E-5

Table S6. The relaxation time fitting parameters of with different relaxation processes

Complex	Fitting Process	Orbach		Raman		QTM	Direct
		τ_0 (s)	U_{eff}	$C(\text{s}^{-1} \text{K}^{-n})$	n	τ_{QTM} (ms)	A
1	QTM+Direct + Orbach	$1.3(1) \times 10^{-7}$	111(2)	-	-	2.9(2)	131(6)
2	QTM+Raman+ Orbach	$1.5(5) \times 10^{-10}$	283(8)	$1.32(6) \times 10^{-4}$	6.21(2)	199(15)	-
3	QTM+Direct + Orbach	$1.3(1) \times 10^{-7}$	108(2)	-	-	2.3(1)	351(7)
4	QTM+Raman+ Orbach	$1.5(10) \times 10^{-10}$	280(15)	$2.40(1) \times 10^{-4}$	6.06(3)	119(4)	-

Table S7. Calculated energy levels (cm^{-1}), \mathbf{g} (g_x , g_y , g_z) tensors and m_J values of the lowest Kramers doublets (KDs) of individual Dy^{3+} fragment of complexes **2** and **4**.

KDs	2		4	
	E/cm^{-1}	g	E/cm^{-1}	g
1	0.0	0.011		0.013
		0.016	0.0	0.018
		19.62		19.71
2	201.9	0.17		0.24
		0.27	211.2	0.38
		16.83		16.71
3	359.9	2.21		10.23
		5.36	363.9	7.02
		11.41		2.88
4	415.8	8.78		1.55
		6.21	421.4	3.99
		0.54		8.75
5	445.9	0.30		1.83
		1.59	476.3	2.53
		16.25		16.51
6	486.4	2.93		1.61
		4.42	500.4	3.10
		11.94		11.20
7	570.4	0.43		0.45
		0.80	599.3	0.76
		15.78		16.09
8	649.4	0.11		0.04
		0.29	697.0	0.13
		18.75		18.65

Table S8. Fitted exchange coupling constant J_{exch} , the calculated dipole-dipole interaction J_{dipolar} and the total J_{total} between Dy^{3+} ions in **2** and **4** (cm^{-1}).

		2	4
J	J_{dipolar}	4.31	4.39
	J_{exch}	-1.5	-2.0
	J_{total}	2.81	2.39

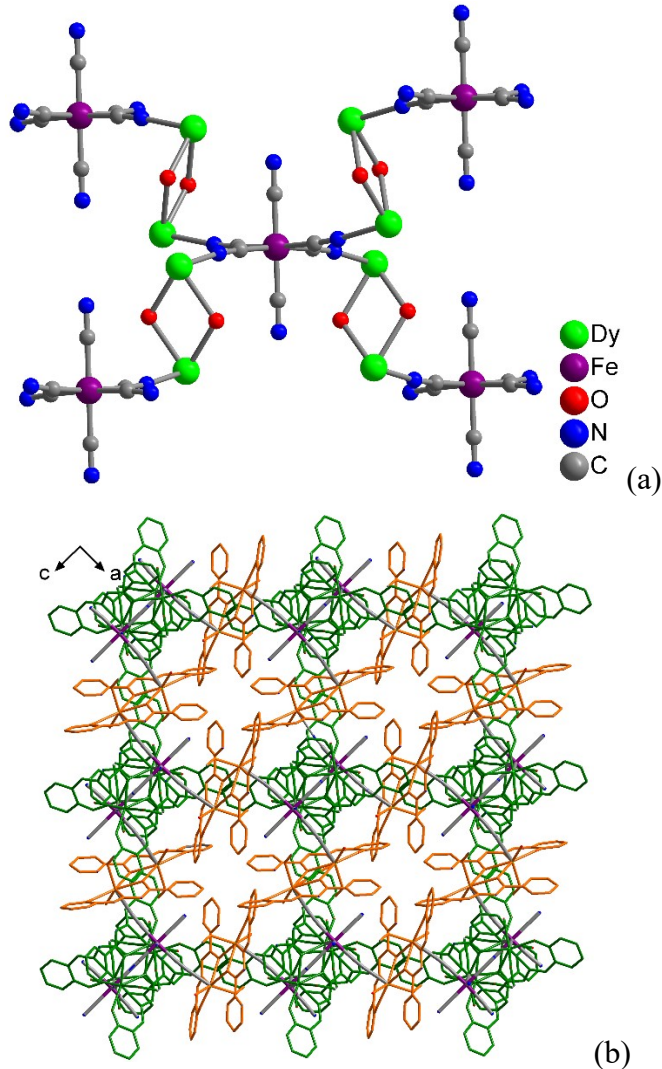


Fig. S1 The connection details between the dimer units and $[Fe(CN)_6]^{3-}$ groups (a) and view of the 3D network along the b direction (b) of complex 1.

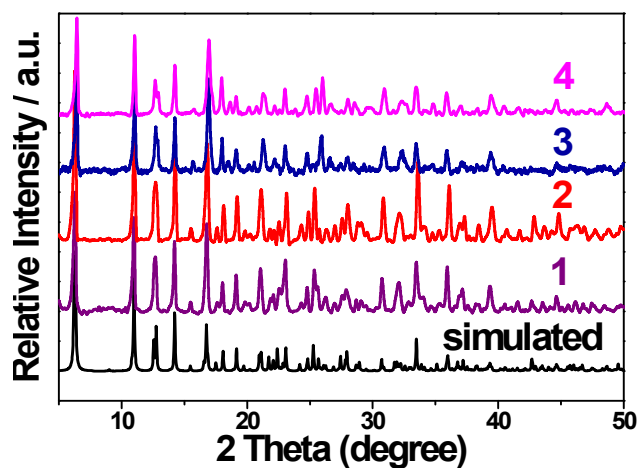


Fig. S2 Powder X-ray diffraction profiles of **1-4** together with simulations from the single crystal data.

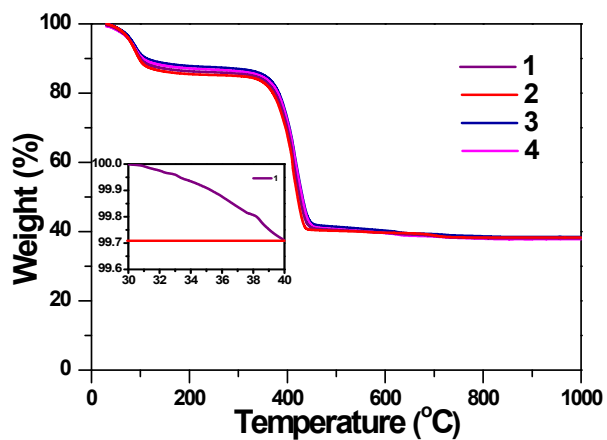


Fig. S3 TGA curves of complex 1-4.

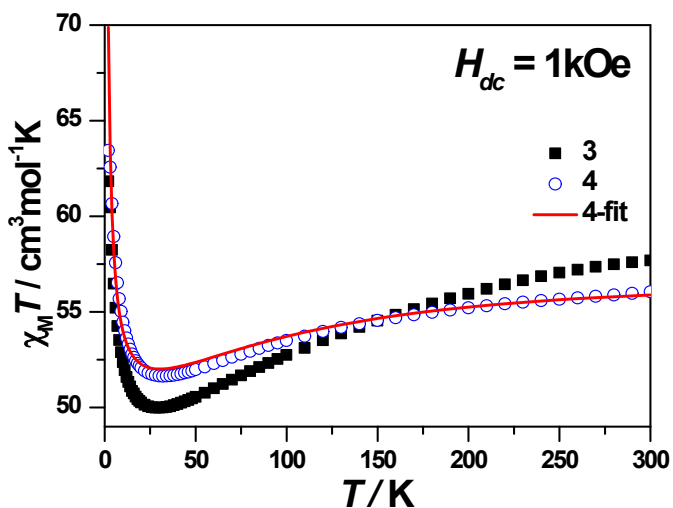


Fig. S4 Temperature dependence of $\chi_M T$ products under 1 kOe dc field for 3 and 4.
The red line is the simulation from *ab initio* calculation.

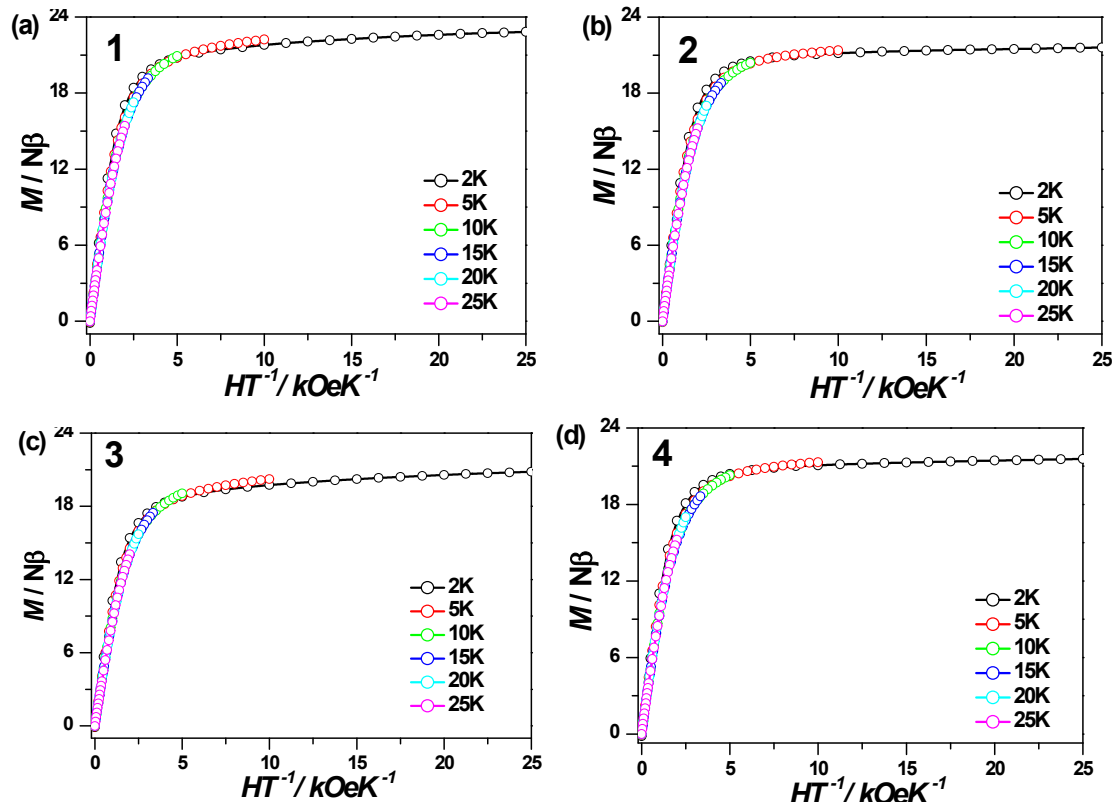


Fig. S5 Plots of $M-H$ for **1-4** at 2, 5, 10, 15, 20 and 15 K.

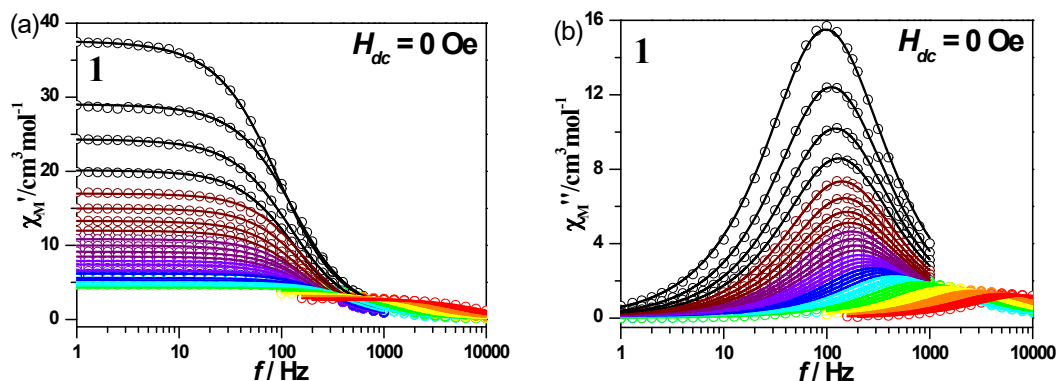


Fig. S6 $Ac-f$ curves measured under 0 kOe dc fields for **1**. Solid lines were fitted using a generalized Debye relaxation model, simultaneously to $\chi'(f)$ and $\chi''(f)$ curves.

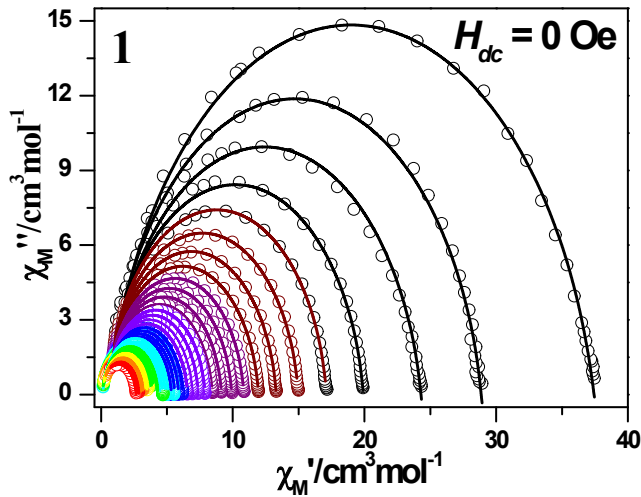


Fig. S7 Cole-cole plots of **1** under 0 kOe *dc* field.

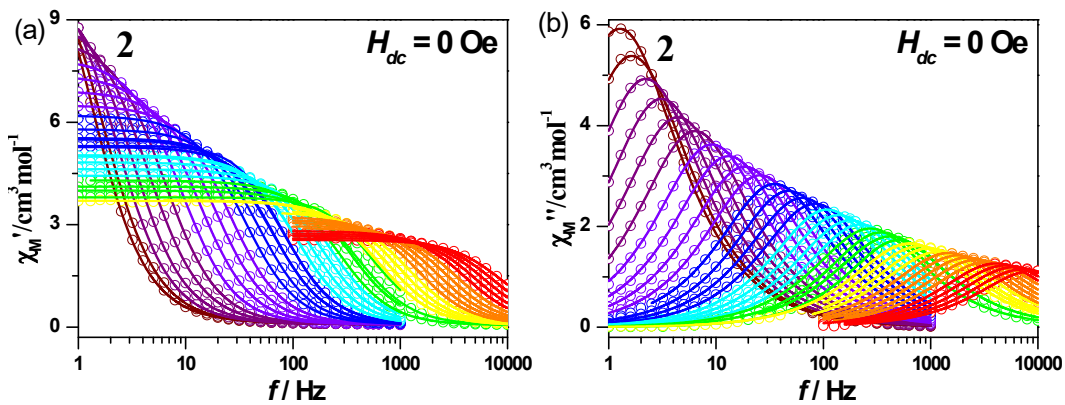


Fig. S8 *Ac*-*f* curves measured under 0 kOe *dc* fields for **2**. Solid lines were fitted using a generalized Debye relaxation model, simultaneously to $\chi'(f)$ and $\chi''(f)$ curves.

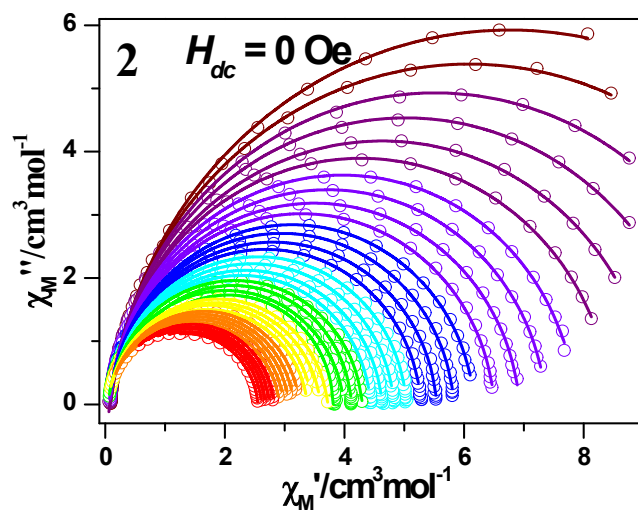


Fig. S9 Cole-cole plots of **2** under 0 kOe *dc* field.

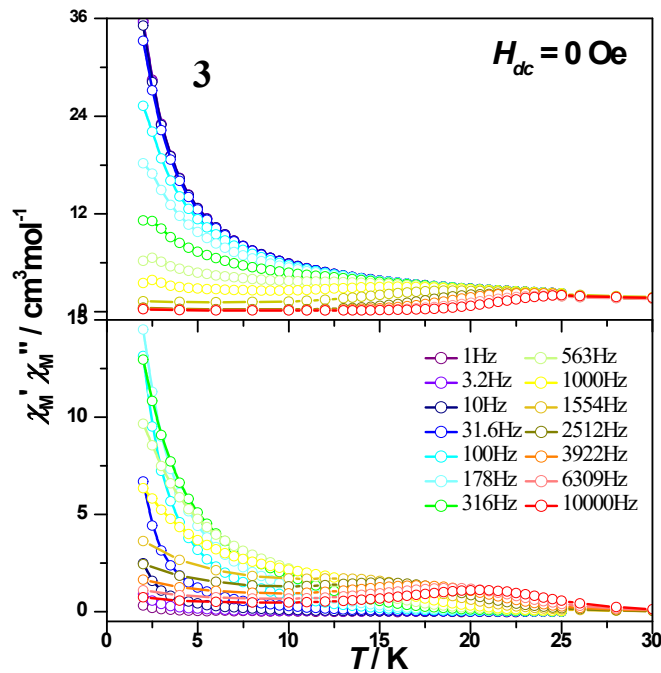


Fig. S10 Temperature dependence of the in-phase (top) and out-of-phase (bottom) ac susceptibility signal under zero field for **3**.

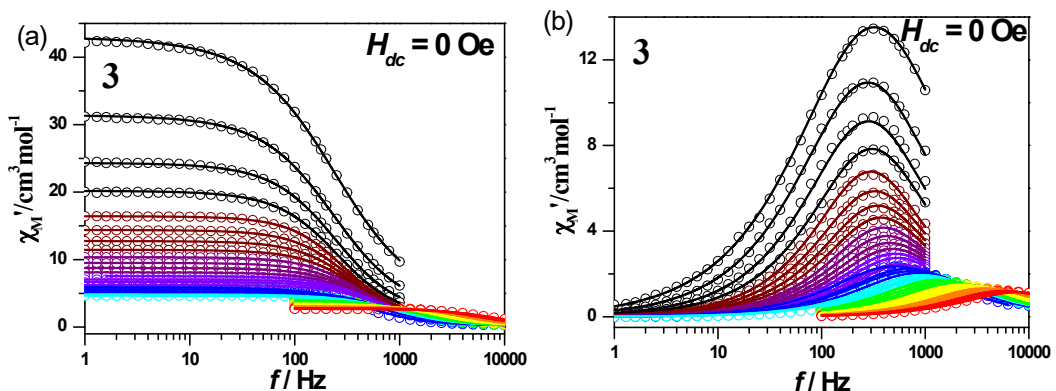


Fig. S11 *Ac-f* curves measured under 0 kOe *dc* fields for **3**. Solid lines were fitted using a generalized Debye relaxation model, simultaneously to $\chi'(f)$ and $\chi''(f)$ curves.

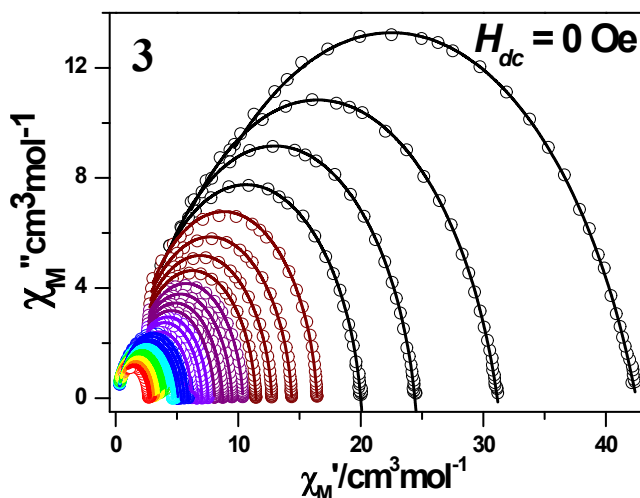


Fig. S12 Cole-cole plots of **3** under 0 kOe *dc* field.

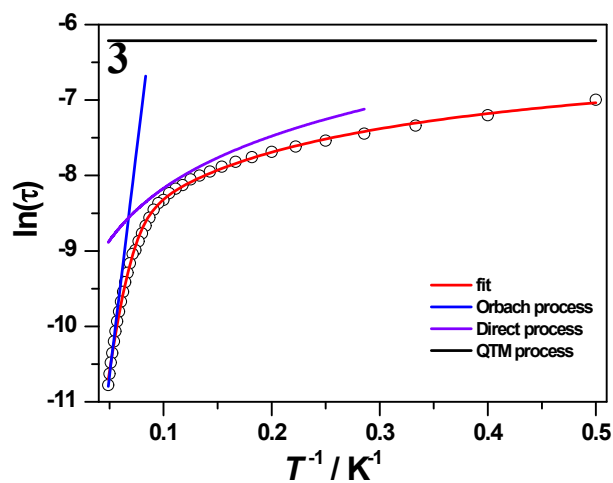


Fig. S13 Plot of $\ln(\tau)$ vs. T^{-1} for **3** under zero dc field.

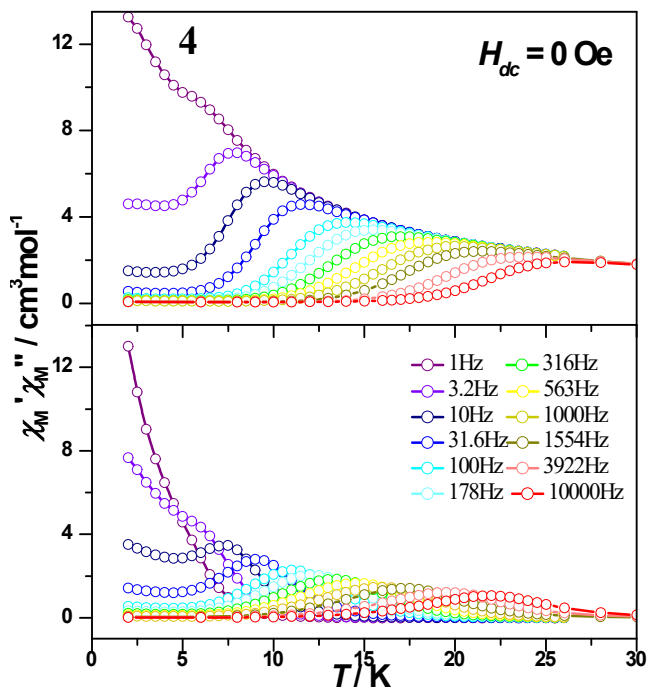


Fig. S14 Temperature dependence of the in-phase (top) and out-of-phase (bottom) ac susceptibility signal under zero field for 4.

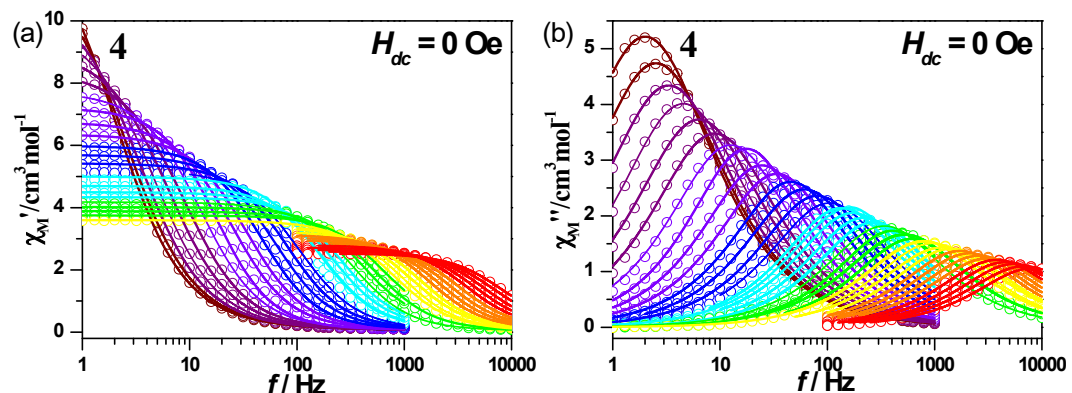


Fig. S15 *Ac-f* curves measured under 0 kOe *dc* fields for 4. Solid lines were fitted using a generalized Debye relaxation model, simultaneously to $\chi'(f)$ and $\chi''(f)$ curves.

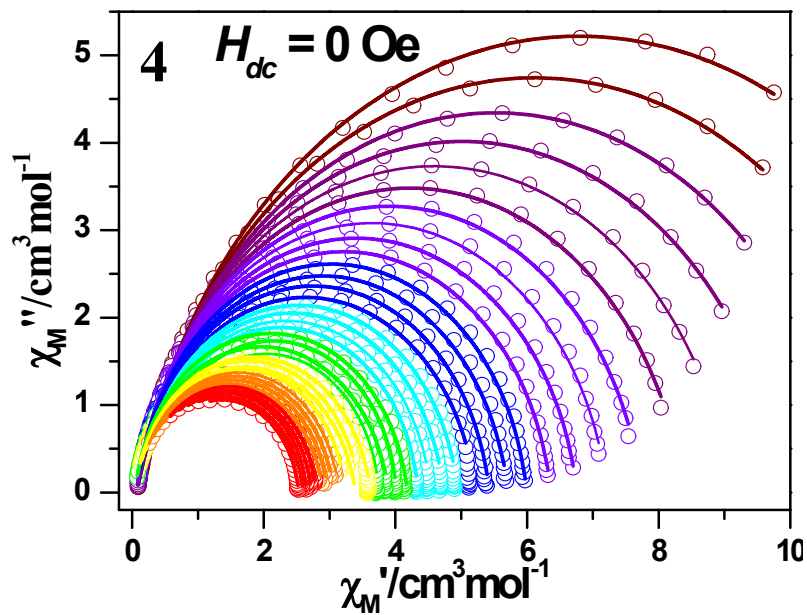


Fig. S16 Cole-cole plots of **4** under 0 kOe *dc* field.

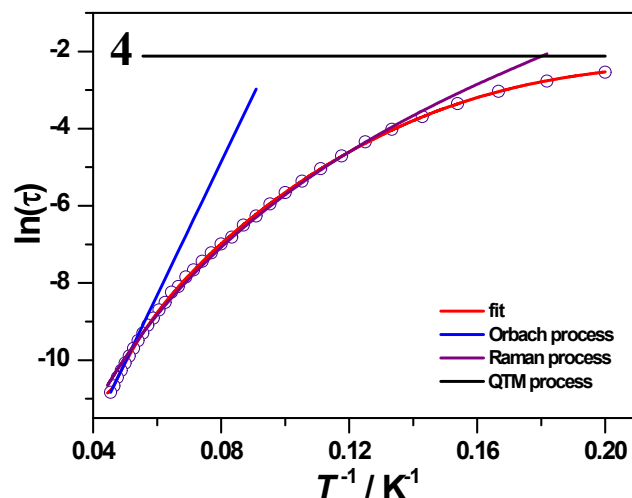


Fig. S17 Plot of $\ln(\tau)$ vs. T^{-1} for **4** under zero dc field.

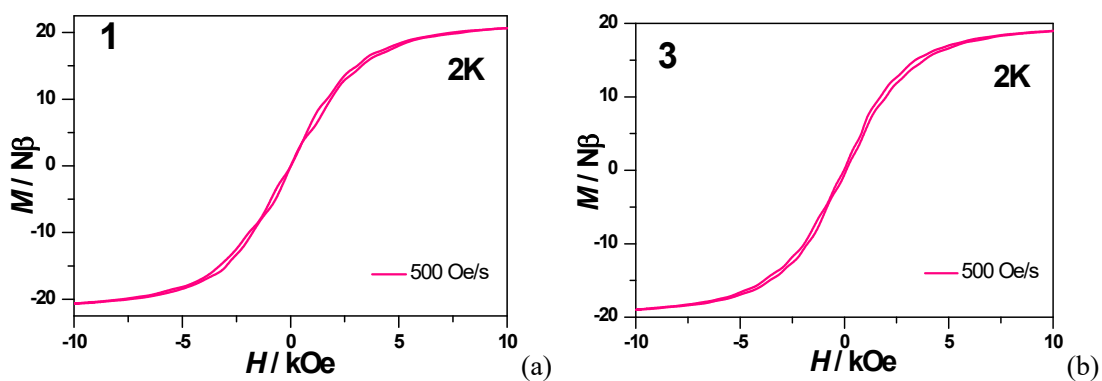


Fig. S18 Hysteresis loop measured with sweeping rates of 500 Oe/s at 2 K for **1** (a) and **3** (b).

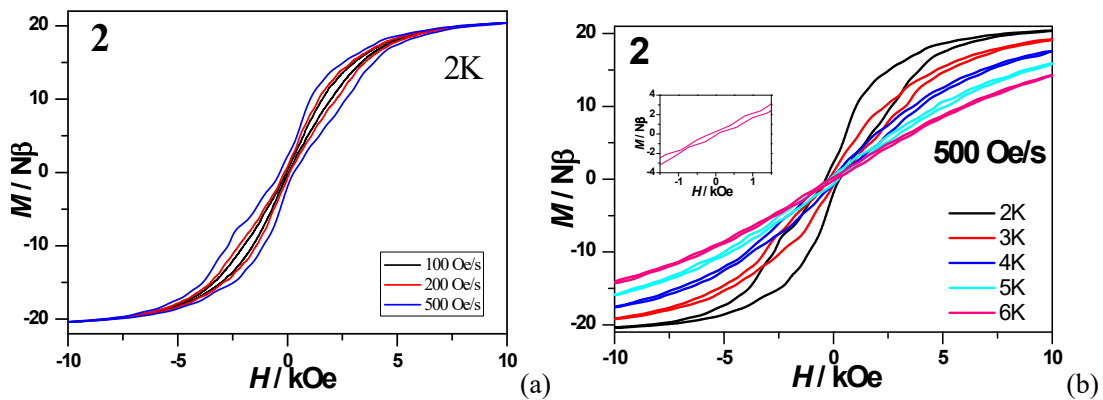


Fig. S19 Hysteresis loop measured with different sweep rates at 2 K (a) and different temperatures with sweeping rates of 500 Oe/s (b) for **2**.

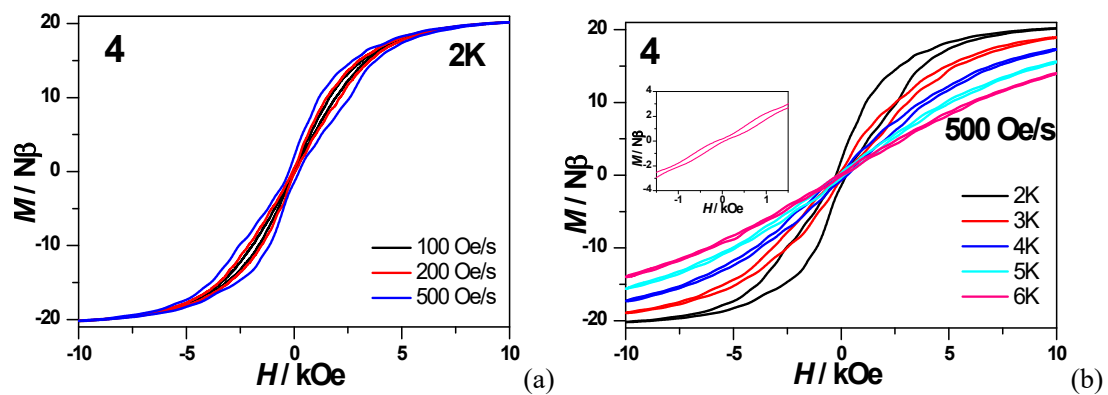


Fig. S20 Hysteresis loop measured with different sweep rates at 2 K (a) and different temperatures with sweeping rates of 500 Oe/s (b) for **4**.

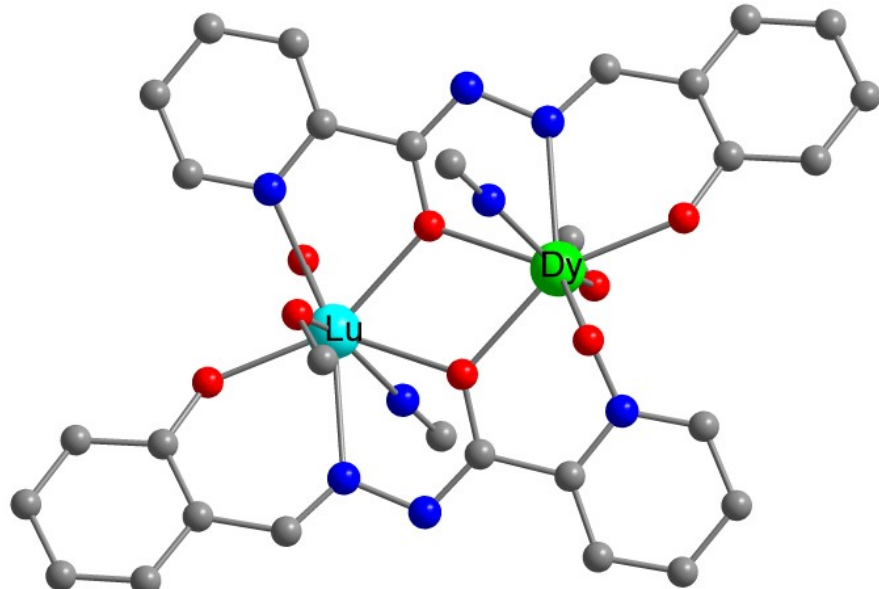


Fig. S21 Calculated model structure of individual Dy^{3+} fragment of complex **2**.

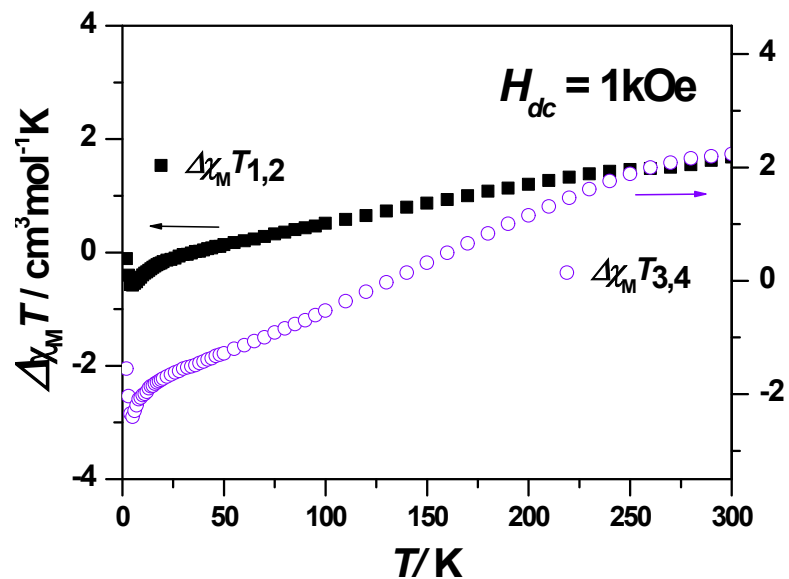


Fig. S22 Temperature dependence of $\Delta\chi_M T$ products under 1 kOe dc field for 1-4.